ELSEVIER

Chemical Engineering Journal 113 (2005) 27–34

Chemical Engineering Journal

www.elsevier.com/locate/cej

Synthesis of Pd/Fe_3O_4 nanoparticle-based catalyst for the cross-coupling of acrylic acid with iodobenzene

Zhifei Wang [a], Bing Shen [b], Zou Aihua [a], Nongyue He [a,*]

[a] *State Key Laboratory of Bioelectronics, Southeast University, 2 Sipailou, Nanjing 210096, PR China*
[b] *Department of Chemistry, Southeast University, 2 Sipailou, Nanjing 210096, PR China*

Received 2 December 2004; received in revised form 11 July 2005; accepted 2 August 2005

Abstract

In this study, catalyst Pd/Fe_3O_4 based on magnetic body with the size of 8 nm was prepared and characterized by TEM, HRTEM, XPS and VSM methods. The results show that Pd^0 atom produced after the first reduction is bound to APTS-coated Fe_3O_4 nanoparticles by the coordination of $–NH_2$ ligand with Pd^0 and then grows into bigger clusters with the increase in the reduction times. However, when the reduction is performed for more than three times, Pd^0 atom produced in subsequent reduction is dispersed in aqueous solution instead of depositing around preexisting Pd^0 atom or clusters. In order to further investigate its catalytic behavior, Heck reaction of the cross-coupling of acrylic acid with iodobenzene was employed. The activity measurements show that the product yield decreased greatly from 81% for the first times to 53% for the fifth times and then kept constant in the subsequent re-use. One of the important reasons for this is that the catalyst aggregates into big particle and becomes more difficult to be dispersed with the increase in reaction times. In a word, this preliminary work provides the primary understanding of the catalyst based on Fe_3O_4 nanoparticles and its application in Heck reaction.

Keywords: Catalysis; Catalyst support; Nanostructure; Separations; Pd/Fe_3O_4; Heck reaction

1. Introduction

In recent years, there are growing interests on the catalytic properties of transition metal nanoparticles because of their large surface area and a great ratio of atoms remaining at the surface [1,2,10]. Although much work has been done [3–8], there is still the paramount challenge for the wide application of transition metal nanoparticles as catalysts in the industry, i.e., how to separate them completely from products. For example, due to the industrial importance of the Heck chemistry, which is traditionally associated with the palladium–phosphine-catalysed reaction of aryl bromides or iodides with olefins and presents one of the simplest ways to obtain various substituted olefins [5], many researches have been focused on designing recyclable catalyst based on Pd nanoparticles [9]. And an advance among those researches is the successful synthesis of dendritic catalyst that can be separated from the reaction medium by the nanofiltration membrane [2–4]. However, such separation does not meet the large-scale application in industry and another problem related to this approach is the leaching of heterogeneous dendritic catalyst [2].

At present, the main idea presented for recyclable systems may be built in liquid–liquid and solid–liquid modes [1]. For a liquid–liquid system, due to the high interfacial tension between water and low-polar organic liquids, the area of the interface is small even with vigorous stirring. Therefore, separation and catalytic efficiency come to a contradiction. Another approach to separate and recycle metal nanoparticles is to immobilize them on solid supports, such as organic polymeric (resin) [10] and inorganic microsphere (Pd/C, Pd/SiO_2, Pd/Al_2O_3, etc.) [1,11], making it really easy and simple to separate the catalyst from the mixtures of the products. However, with solid catalysts suspended within liquids, the transport of reactants within the liquid to the catalyst bodies as well as the transport of them within porous catalyst bodies would be rate limiting, because the transport rate to

* Corresponding author. Tel.: +86 25 83792245; fax: +86 25 83619983.
E-mail address: nyhe1958@163.com (N. He).

1385-8947/$ – see front matter © 2005 Elsevier B.V. All rights reserved.
doi:10.1016/j.cej.2005.08.003

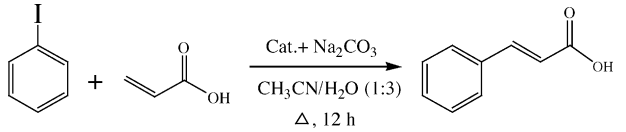

Scheme 1. Heck reaction of the cross-coupling of acrylic acid with iodobenzene.

the surface of the catalyst bodies is proportional to $1/D$ (D is the diameter of catalyst body) [12]. To raise the rate of the reaction, it is therefore attractive to utilize small catalyst bodies.

Because the conventional centrifugation or filtration, which calls for the particle with the size of at least about 3 μm, cannot be applied to separate the catalyst bodies of the nanometer size [12], it is necessary to develop new procedure, such as magnetic separation. However, there are two difficulties with the utilization of magnetic bodies as the catalyst supports, viz., the magnetostatic attraction between ferromagnetic particles and the effect of their surface properties on the catalyst.

To overcome the above deficiencies, we chose Fe_3O_4 nanoparticles with the size of 8 nm as the catalyst body. Before the preparation of the catalyst Pd/Fe_3O_4, its surface was firstly modified with the 3-aminopropyl triethoxysilane (APTS). And then the catalytic site Pd^0 was bound to the surface of Fe_3O_4 nanoparticles by means of the coordination of $–NH_2$ ligand with Pd^0. Finally, the catalytic behavior of Pd/Fe_3O_4 nanoparticles was measured by the Heck reaction of the cross-coupling of acrylic acid with iodobenzene (please see Scheme 1).

2. Experimental

2.1. Material

All chemicals used are of analytical grade from Shanghai Chemical Reagent Corporation, except for iodobenzene, which is chemical grade. Water used in the experiments was deionized (DI), doubly distilled and deoxygenated prior to use.

2.2. Preparation of Fe_3O_4 nanoparticle

Fe_3O_4 nanoparticle was prepared by the conventional coprecipitation method. Firstly, 5.2 g of $FeCl_3$, 2.0 g of $FeCl_2$ and 0.85 mL of 12 mol/L HCl were dissolved in 25 mL of DI water under N_2 protection. And then the resulting solution was added drop-wise into 250 mL of 1.5 mol/L NaOH solution under vigorous stirring. After the reaction, the obtained precipitate was separated from the reaction medium under the magnetic field and washed with DI water for three times and ethanol for two times. Finally, a portion of Fe_3O_4 nanoparticles was dispersed in ethanol with the concentration of 5 g/L.

2.3. APTS-coated Fe_3O_4 nanoparticle

The modification of Fe_3O_4 nanoparticles with 3-aminopropyl triethoxysilane was performed in ethanol solution at room temperature and a small amount of water was added to accelerate to its hydrolysis. Typically, 25 mL of the above ethanol solution with 5 g/L of Fe_3O_4 nanoparticles was diluted to 150 mL with ethanol and 1 mL of H_2O. In order to disperse Fe_3O_4 nanoparticle well, the solution was further treated by ultrasonic wave for 30 min. After that, 0.4 mL of APTS was added with rapid stirring, and then the reactant mixture was stirred for another 7 h. Finally, the APTS-coated Fe_3O_4 nanoparticles were separated from the mixture by the ultracentrifugation and washed with ethanol for five times. Before the next step, the APTS-coated Fe_3O_4 nanoparticles were dispersed in ethanol with the concentration of 1 g/L.

2.4. Preparation of catalyst Pd/Fe_3O_4

Catalyst Pd/Fe_3O_4 was prepared by refluxing the reactant mixture of H_2PdCl_4 solution, APTS-coated Fe_3O_4 nanoparticles and ethanol, and Pd^{2+} ion was reduced by the ethanol. In the first reduction, a mixture of 15 mL of ethanol containing APTS-coated Fe_3O_4 nanoparticles (1 g/L) as prepared above, 14 mL of 0.6 mmol/L H_2PdCl_4 solution and 21 mL of H_2O was refluxed for 3 h in air. With the progress of the reaction, the color of the solution turned from yellow to black. After the reaction, catalyst Pd/Fe_3O_4 was separated from the reaction medium under the magnetic field and the residual solution looked colorless. For the convenience of the discussion, the obtained catalyst was tagged as Pd/Fe_3O_4 after the first reduction.

In order to deposit more Pd^0 on the surface of Fe_3O_4 nanoparticles, the mixture of Pd/Fe_3O_4 particle obtained in the first reduction, 14 mL of 0.6 mmol/L H_2PdCl_4 solution, 15 mL of ethanol and 21 mL of H_2O was refluxed again. And the obtained product was tagged as Pd/Fe_3O_4 after the second reduction. The above process was repeated until the residual solution after the removal of Pd/Fe_3O_4 appeared brown and the product was tagged according to the corresponding times of the reduction. We found when the times of reduction was more than three, the residual solution started to look brown, which indicates that after the reaction, Pd^0 was dispersed in the solution instead of depositing on the surface of Fe_3O_4 nanoparticles.

2.5. General procedure for the catalytic tests

The catalytic behavior of Pd/Fe_3O_4 nanoparticles was measured by employing the cross-coupling of acrylic acid with iodobenzene. In the typical reaction, 1 eq. (4 mmol) of iodobenzene, 2 eq. (8 mmol) of acrylic acid, 15 mg of catalyst Pd/Fe_3O_4, 20 mL of a CH_3CN solution and 2.5 eq. (10 mmol) of anhydrous Na_2CO_3 were added to 60 mL of water. And the mixture was refluxed for 12 h. After the reaction, catalyst Pd/Fe_3O_4 was separated from the reaction medium by

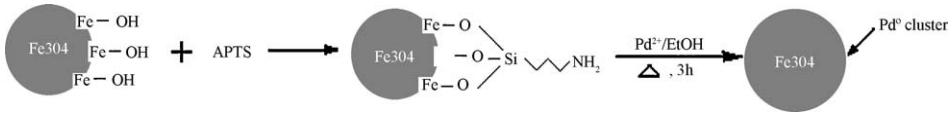

Scheme 2. Procedure of the preparation of catalyst Pd/Fe_3O_4.

the magnetic field and left for the next reaction. Five millilitres of 5% HCl was then added to the residual solution, from which white solid was formed. Finally, the solid was filtered, washed several times with fresh water and then recrystallized by water–ethanol (3:1) solution.

Before the re-use in the next reaction, Pd/Fe_3O_4 was thoroughly washed under the ultrasonic wave. With the increase in times of the reaction, we found that the catalyst Pd/Fe_3O_4 had aggregated into bigger particles and became more difficult to be dispersed in the reaction medium.

2.6. Characterization

The particle size and morphology of the samples were determined by transmission electronic microscopy (TEM) with JEM-200CX operating at 200 kV. HRTEM images were obtained by employing a JEOL-4000EX high-resolution transmission electron microscope with a 400 kV accelerating voltage. The surface composition of catalyst Pd/Fe_3O_4 was detected by the X-ray photoelectron spectra (XPS) recorded on an ESCALAB MKII, using a non-monochromatized Mg Kα X-ray as the excitation source and choosing C (1s) (284.6 eV) as the reference line. The infrared spectra of APTS-coated Fe_3O_4 nanoparticles were recorded on a Nicolet 170 SX Fourier transform infrared spectrometer (FT-IR) using KBr pellets. Magnetization measurements of both APTS-coated Fe_3O_4 nanoparticles and catalyst Pd/Fe_3O_4 were performed at room temperature using vibration sample magnetometer (VSM).

3. Results and discussion

3.1. Study of the preparation of catalyst Pd/Fe_3O_4

Catalyst Pd/Fe_3O_4 is prepared by ligand-mediated immobilization of metal atom on functionalized oxide surfaces as shown in Scheme 2. It can be found that the surfaces of Fe_3O_4 nanoparticles are firstly modified with APTS, and then Pd^0 atom from the reduction of Pd^{2+} by the ethanol was bound to the surface through the pendent amine group. In comparison with other reductants, such as $N_2H_4{\cdot}H_2O$, $NaBH_4$, etc., ethanol is the weak reducing agent. So, the formation of Pd atoms is gentle and the atoms have enough time to deposit on the surface of Fe_3O_4 nanoparticles. The amount of Pd^0 deposited on the surface is controlled by the times of the reduction. In the experiment, we found that when the times of the reduction is more than three, the residue solution looked brown after the removal of Pd/Fe_3O_4, indicating that at this time, the deposition of Pd^0 on the surface reaches the saturation and the redundant Pd^0 stays in the solution. In the typical experiment, the mass concentration of Fe_3O_4 nanoparticle is 1 g/L and its mole concentration can be calculated by the following formula (1). The number of Fe atom in every Fe_3O_4 nanoparticle can be calculated by means of the formula (2), where $V_{Fe_3O_4}$ refers to the:

$$\text{mole concentration}_{Fe_3O_4} = \frac{\text{mass concentration}_{Fe_3O_4}}{N_{Fe} \times 77.3} \quad (1)$$

$$N_{Fe} = \frac{4/3\pi R^3 Na}{V_{Fe_3O_4}} \times 3 = 10855 \quad (2)$$

molar volume of bulk Fe_3O_4, R the mean radius of Fe_3O_4 nanoparticles and Na is Avogadro's number. So, its mole concentration is about 1.2×10^{-6} mol/L [13]. During the preparation of catalyst, Pd/Fe_3O_4 nanoparticles can be stably dispersed in the aqueous solution due to the remainder electrostatic repulsion on the surface of Fe_3O_4.

For Fe_3O_4 nanoparticles dispersed in a neutral aqueous solution, the bare atoms of Fe and O on the particle surface would adsorb OH^- and H^+, respectively. As a result, there are many –OH groups around the surface of Fe_3O_4 nanoparticles. In addition, because the reaction between –OH on the surface and APTS can easily take place, APTS is usually employed to modify the surface of metal oxide. Fig. 1 shows FT-IR spectrum of APTS-coated Fe_3O_4 nanoparticles. In comparison with the standard spectra, following absorption bands can be observed: bands at 2926.8 and 2853.8 cm^{-1} due to the

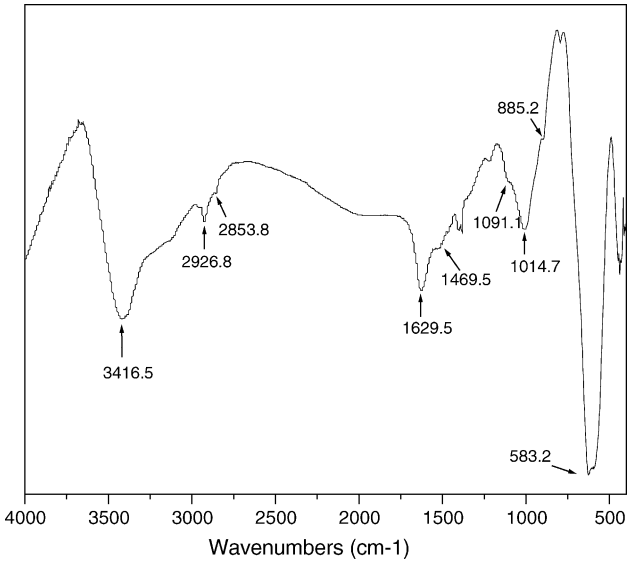

Fig. 1. FT-IR spectrum of APTS-coated Fe_3O_4 nanoparticles.

stretching vibration of C–H bond, band at 1014.7 cm^{-1} due to the stretching vibration of Si–O bond, band at 1091.1 cm^{-1} due to the stretching vibration of C–N bond and band at 885.2 cm^{-1} due to the bending vibration of $–NH_2$ bond. Moreover, the absorption bands at 3416.5 and 1629.5 cm^{-1} could be attributed to the co-contribution of $–NH_2$ bond and remainder water in the sample [13]. All of those bands reveal that the surface of Fe_3O_4 nanoparticles is successfully modified with APTS. Representative TEM image of APTS-coated Fe_3O_4 nanoparticles is shown in Fig. 2, from which it can be seen that most of the particles are quasi-spherical with an average diameter of 8 nm.

Fig. 3 shows TEM results of catalyst Pd/Fe_3O_4 after the third reduction, and A, B and C represent images of TEM, HRTEM and its corresponding diffraction pattern, respectively. In comparison with APTS-coated Fe_3O_4 nanoparticles, the average size of catalyst Pd/Fe_3O_4 is about 8 nm and no obvious morphological change is observed after the deposition of Pd^0, indicating that the deposition of Pd^0 atom is not enough to increase the size of the particle. In addition, we did not find the free Pd^0 nanoparticle around Fe_3O_4 nanoparticles by TEM. The above results can be further confirmed by the lattice-resolving image (Fig. 3B), which shows that catalyst Pd/Fe_3O_4 is nanocrystalline and there is no obvious deposition of Pd^0 around the surface. The selected area diffraction pattern (C) of Fig. 3 is the ring pattern, which is characteristic of the cubic structure of Fe_3O_4 compared with the theoretic values. So, we presume that the amount of Pd^0 on the surface is not enough to form the obvious shell around Fe_3O_4 nanoparticle.

In order to understand the surface variation of catalyst Pd/Fe_3O_4 with the increase in the times of reduction, XPS characterization was employed. Fig. 4 shows the full XPS patterns, and a, b and c represent catalyst Pd/Fe_3O_4 after the first, the second and the third reduction, respectively. The band at about 340 eV can be attributed to the binding energy of Pd 3d. It can be seen that the spectrum area of Pd 3d increases with the increase in times of reduction. Fig. 5A–C further shows XPS patterns of Pd 3d of catalyst Pd/Fe_3O_4 after the first, the second and the third reduction, respectively, and the corresponding spectrum data are listed in Table 1. For cata-

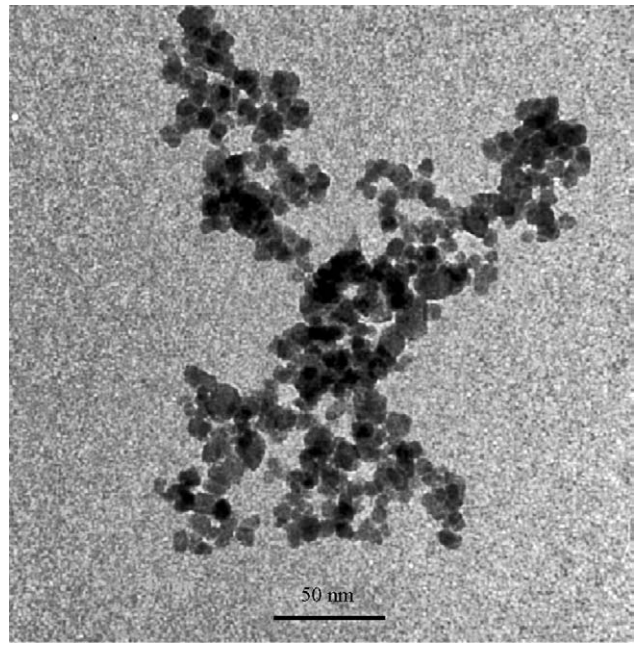

Fig. 2. A TEM image of APTS-coated Fe_3O_4 nanoparticles.

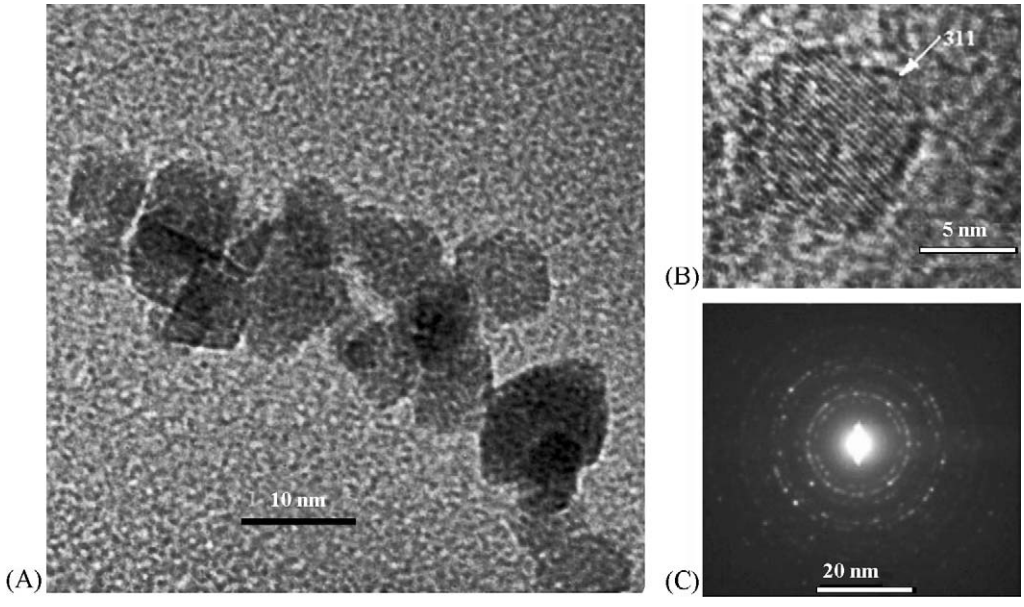

Fig. 3. (A) A TEM image of catalyst Pd/Fe_3O_4 after three times reduction. (B) A HRTEM image of the nanoparticles. The lattice spacing for (3 1 1) is 0.24 nm. (C) Its corresponding diffraction pattern.

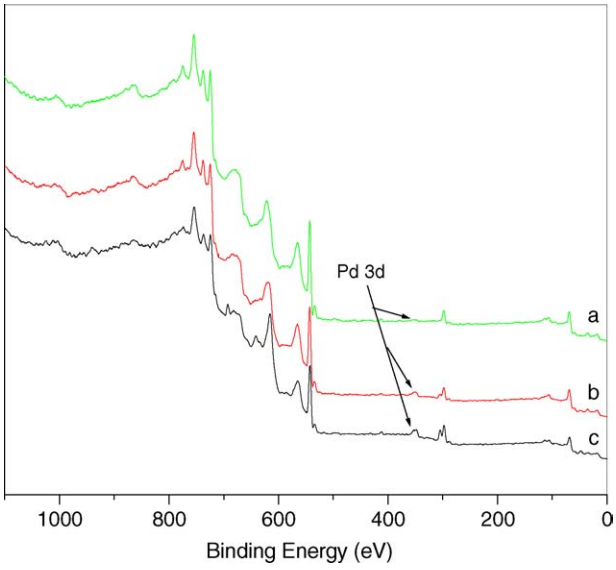

Fig. 4. Full XPS spectra of catalysts Pd/Fe_3O_4 with the different times of reduction; a, b and c represent the catalyst after the first, the second and the third reduction, respectively.

lyst Pd/Fe_3O_4 after the first reduction, we find that it consists of the peaks at 339.1 and 339.9 eV due to Pd $3d_{3/2}$ and the band at about 334 eV that can be further resolved into two peaks at 334.3 and 335.0 eV due to Pd $3d_{5/2}$. In comparison with the standard binding energy (Pd^0 with Pd $3d_{5/2}$ of about 335 eV) [14], it can be concluded that these peaks should be assigned into two Pd^0 species: (334.3, 339.1 eV) and (335.0, 339.9 eV). As we known, the position of Pd 3d peak is usually influenced by the local chemical/physical environment around Pd species besides the formal oxidation state and shifts to lower binding energy when the charge density around it increases [14]. So, the peaks at (334.3, 339.1 eV) should be due to Pd^0 species bound directly to $-NH_2$ ligand, and the peaks at (335.0, 339.9 eV) should be due to another Pd^0 species in the body of Pd^0 cluster. The contribution of the charge transfer of $-NH_2$ ligand to Pd^0 results in the increase in the charge density around Pd^0 and the decrease in binding energy. For catalysts Pd/Fe_3O_4 after the second or third reduction, only two main peaks are observed and Pd $3d_{5/2}$ positions are at 334.8 and 334.9 eV, respectively, which can be assigned to Pd^0 species in the body of Pd^0 cluster. When comparing the above value with those of Pd/Fe_3O_4 after the first reduction, it can be found that with the increase

Table 1
Pd $3d_{5/2}$ and Pd $3d_{3/2}$ position of catalyst Pd/Fe_3O_4 with the different times of reduction

Catalysts	Pd $3d_{5/2}$ position (eV)	Pd $3d_{3/2}$ position (eV)
After the first reduction	(a) 335.0	339.9
	(b) 334.3	339.1
After the second reduction	334.8	340.3
After the third reduction	334.9	340.2

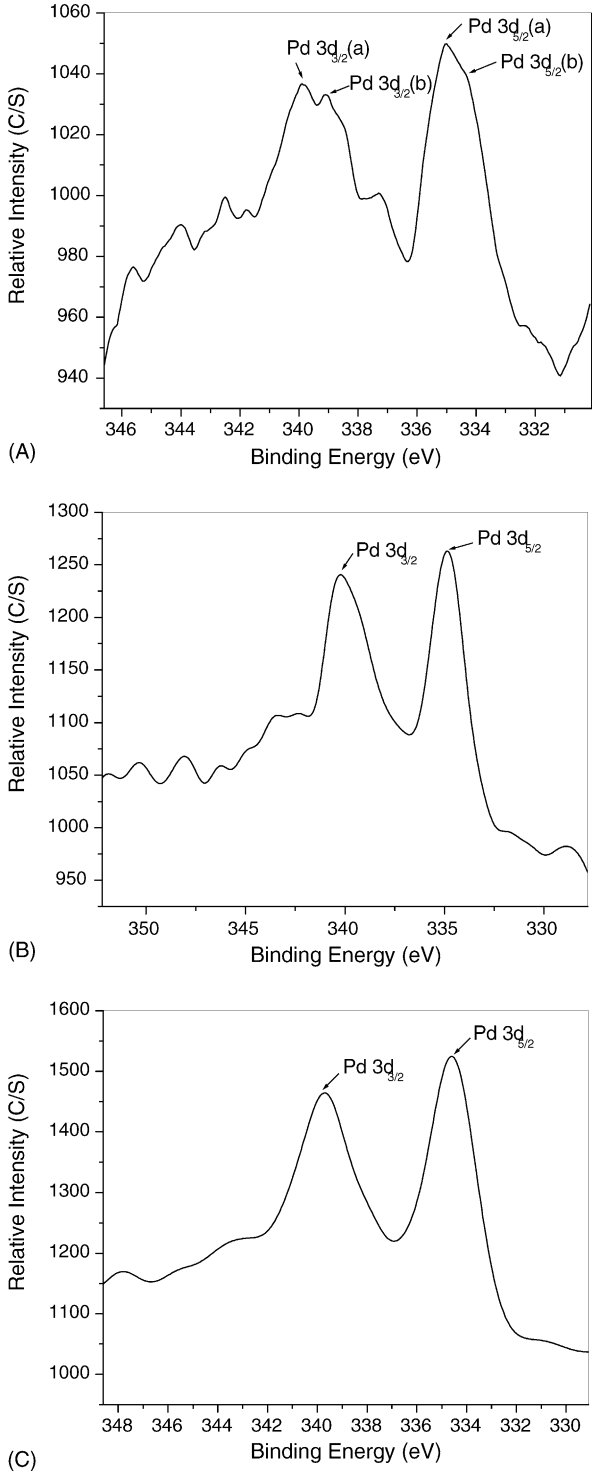

Fig. 5. XPS spectra of Pd 3d of catalysts Pd/Fe_3O_4 with the different times of reduction. A, B and C represent the catalyst after the first, the second and the third reduction, respectively.

in times of reduction, the content of Pd^0 species that coordinates with $-NH_2$ ligand on the surface decreases and most of Pd^0 species is in the body of Pd^0 cluster. The above results indicate that after the first reduction, Pd^0 atoms is bound to APTS-coated Fe_3O_4 nanoparticles through the coordination

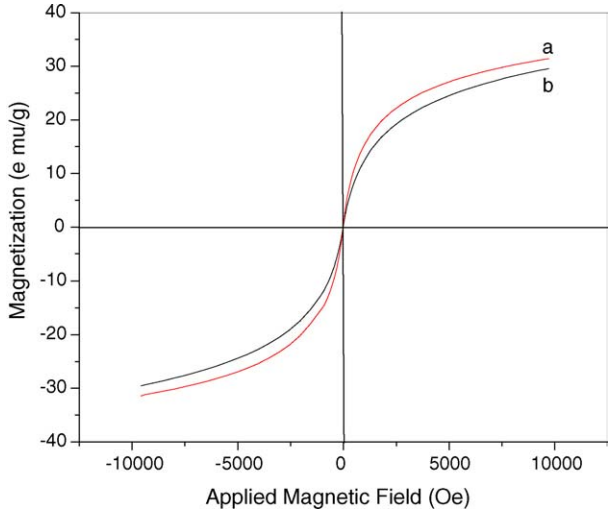

Fig. 6. Magnetization curves obtained by VSM at room temperature: (a) APTS-Fe_3O_4 and (b) Pd/Fe_3O_4.

of $-NH_2$ ligand with Pd^0 and then grows into bigger clusters when the reduction is performed more, which can be proved by the peak area and the position of Pd $3d_{5/2}$. Combining the above results with the one from TEM characteristic (see Fig. 3), it can be concluded that after the reduction, Pd^0 on the surface of catalyst Pd/Fe_3O_4 mainly exists as monatomic or clusters and grows into very small amorphous particles formed by several atoms with the increase in times of reduction. The element analysis of catalyst Pd/Fe_3O_4 after the third reduction by the flame atomic absorption spectroscopy (AAS) indicated that the content of palladium is about 0.6%.

Fig. 6 shows the magnetization curves of the APTS-coated Fe_3O_4 (a) and catalyst Pd/Fe_3O_4 after the third reduction (b). It can be seen that in comparison with 31.4 emu/g of APTS-coated Fe_3O_4, the saturation of catalyst Pd/Fe_3O_4 is 29.6 emu/g after coated by Pd. The difference between them indicates that a small amount of Pd^0 was bound to the surface of APTS-coated Fe_3O_4 nanoparticles. There is no hysteresis, and both remanence and coercivity are zero, suggesting that such nanospheres are superparamagnetic.

3.2. Catalytic activity of Pd/Fe_3O_4

Herein, the catalytic activity of Pd/Fe_3O_4 was investigated by the cross-coupling of acrylic acid with iodobenzene (one of the Heck reactions). H_2O/CH_3CN (3:1) was used as the reaction medium due to environmental, economical and safety reasons. Na_2CO_3 was used to neutralize the acid (HX) ensuing from the formal exchange of a hydrogen atom with an aryl group. The experiment process has been described in Section 2, and besides cinnamic acid, no other byproducts were detected. All of the products were further confirmed by the determination of the melting point (133 °C) and ^1H NMR.

3.2.1. Effect of the times of reduction on the catalytic activity of Pd/Fe_3O_4

Table 2 shows the effect of the times of reduction on the catalytic activity of Pd/Fe_3O_4, and TON can be estimated as (moles of coupling products) × (moles of catalyst Pd/Fe_3O_4)$^{-1}$. Those data clearly demonstrate that pure APTS-coated Fe_3O_4 without the deposition of Pd^0 has no activity. Also, it can be seen that TON firstly increases with the increase in times of reduction, reaches the maximum 180,000 when the times of reduction is three and then keeps constant after the third reduction, which can be explained by the variation of Pd^0 content or its peak position got from XPS results. From them, it can be found that after the first reduction, the content of Pd^0 is small and most of Pd^0 is bound to $-NH_2$ ligand. When the times of reduction increases, Pd^0 produced in subsequent reduction deposits around preexisting Pd^0 atom and clusters into very small amorphous particles formed by several atoms. In this process, it can be envisioned that the active sites for catalyst increase with the increase in times of reduction, leading to the increase of TON. The failure to increase the yield with reduction times more than three can be attributed to the failure of deposition of more Pd^0 atom produced in subsequent reduction around preexisting Pd^0 atom. As mentioned in Section 2, the residual solution after the removal of Pd/Fe_3O_4 nanoparticles from reaction medium appeared brown when the reduction was performed more than three times, which indicates that the formed Pd^0 is dispersed in aqueous solvent instead of depositing on the surface of Fe_3O_4 nanoparticles. From the above results, it can be concluded that palladium catalyst based on the magnetic body with the size of 8 nm has good performance and Fe_3O_4 as the support has no obvious inhibitory action on the activity of Pd^0, which builds up the good ground for the future research. In addition, it can be found that Pd^0 species, which are either monatomic or clustered into very small amorphous particles formed by several atoms, must be and really are very active.

3.2.2. Product yield as a function of cycle

Fig. 7 shows the variation of product yield with the times of cycle, and it can be seen that the activity decreased greatly from 81% for the first times to 53% for the fifth times and

Table 2
Product yield of catalyst Pd/Fe_3O_4 with the different times of reduction

Entry	Catalyst	Yield (%)	TON	TOF (h^{-1})
0	Without the reduction	0	0	0
1	After the first reduction	42	93333	7777
2	After the second reduction	74	164444	13703
3	After the third reduction	81	180000	15000
4	After the fourth reduction	80	177777	14814
5	After the fifth reduction	80	177777	14814

Reaction conditions: 4 mmol of iodobenzene, 8 mmol of acrylic acid, 15 mg of catalyst Pd/Fe_3O_4, 20 mL of a CH_3CN solution and 10 mmol of anhydrous Na_2CO_3 were added to 60 mL of water, reflux for 12 h. TON: moles of coupling products/moles of catalyst Pd/Fe_3O_4; TOF: moles of coupling products/moles of catalyst Pd/Fe_3O_4 per hour.

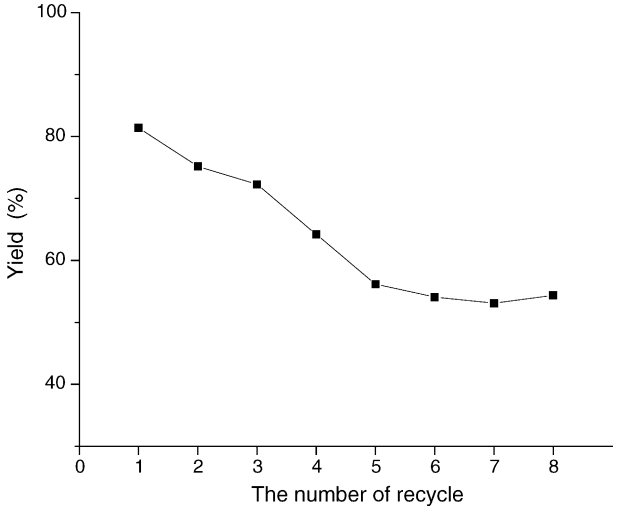

Fig. 7. Product yield as a function of the times of cycle.

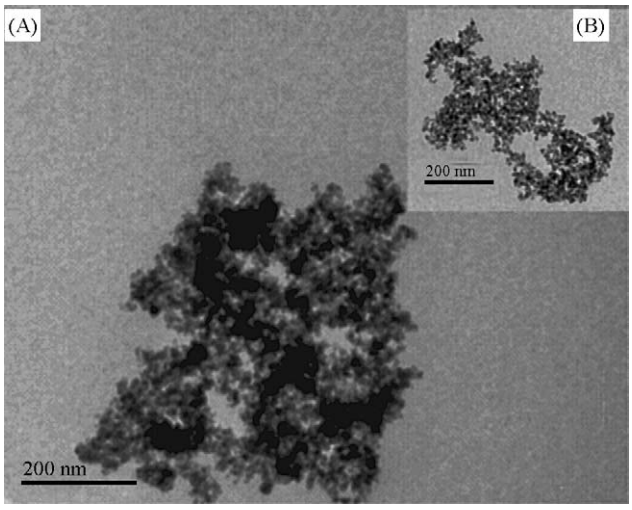

Fig. 8. TEM images of catalyst Pd/Fe_3O_4 after the reaction for five times cycle (A) and before the reaction (B).

then kept constant in the subsequent re-use. According to the possible mechanism involved in the reaction [8], Pd^0 atom is firstly released as the consequence of the oxidative addition of halide to the surface Pd^0 atoms and then redeposited on the surface. So, the leaching of Pd^0 usually is one of the critical factors that result in the loss of the activity during the re-use. However, the results from flame atomic absorption spectroscopy show that the amount of palladium in the residual solution after each reaction is too low to be detected, suggesting that the loss of activity cannot be contributed to the leaching of Pd^0. Since the Pd leaching and redeposition may depend on the state of Pd dispersion (particle size and metal–support interactions) and/or the surface properties of support, the preparation of catalyst is crucial to prevent the Pd leaching. As described above, Pd/Fe_3O_4 used here is prepared by the coordination link of Pd^0 with $–NH_2$ ligand and the amount of Pd^0 in the catalyst is small, resulting in that Pd^0 is strong bound to the surface of Fe_3O_4 nanoparticle. So, that is why no obvious leaching of Pd was observed in re-use.

In order to understand the cause resulting in the loss of activity in re-use, Fig. 8 further shows TEM images of catalyst Pd/Fe_3O_4 after the reaction for five times cycle (A) and before the reaction (B). It can be seen that after the reaction for five times cycle, Pd/Fe_3O_4 nanoparticles aggregate into the big particle in contrast with the clear dispersion of them before the reaction. In addition, this can be proved by the experiment phenomenon that the dispersion of catalyst Pd/Fe_3O_4 became more difficult in the reactant mixture even under the ultrasonic wave with the increase in the times of reaction. The above results indicate that with the increase in times of reaction, the aggregation of catalyst Pd/Fe_3O_4 becomes more seriously even after the thorough washing, which results in the decrease in the surface area of the catalyst. As we known, the activity of the catalyst is usually proportional to its surface area. If the area of the interface between Pd/Fe_3O_4 and the reactant decreases due to the conglomeration of particles, the corresponding catalytic activity will decrease. So, the aggregation of catalyst Pd/Fe_3O_4 will be responsible for the loss of the activity of Pd/Fe_3O_4 in re-use.

4. Conclusion

As mentioned above, recovery and recycling of expensive metal nanoparticle catalyst, such as palladium, is a major development issue besides its activity. In this work, we synthesized the new catalyst based on the superparamagnetic body with the size of 8 nm, with the attempts to understand the catalysis behavior in the re-use by the cross-coupling of acrylic acid with iodobenzene. The results of TEM, HRTEM, IR, XPS and VSM characteristic show that Pd^0 atom produced after the first reduction is bound to APTS-coated Fe_3O_4 nanoparticles by the coordination of $–NH_2$ ligand with Pd^0 and then grows into bigger clusters with the increase in times of the reduction. However, when the times of reduction is more than three, Pd^0 atom produced in subsequent reduction is dispersed in aqueous solution instead of depositing around preexisting Pd^0 atom or clusters. So, it is difficult to find the obvious core shell structure during the preparation of catalyst Pd/Fe_3O_4.

The activity measurement of catalyst Pd/Fe_3O_4 shows that pure APTS-coated Fe_3O_4 nanoparticles have no activity for the reaction of acrylic acid with iodobenzene and the active site is related to Pd^0 atoms or cluster deposited at the surface of Fe_3O_4. Also, it can be seen that the catalyst has the good performance with TOF of 15,000 in the first reaction as compared with other catalysts supported on silica, alumina and carbon [15]. Whereas the activity in re-use was poor, considering the reduction in activity with the times of reaction increasing. One of the important reasons for this is that the catalyst aggregates into big particle and become more difficult to be dispersed with the increase in times of reac-

tion, which results in the reduced surface area of the catalyst. Moreover, no leaching of Pd^0 was detected in the residual solution.

So, it is necessary to pay more attention to the improvement of the stability or the preparation method of catalyst Pd/Fe_3O_4 considering its good performance in the first reaction and easy separation from the reaction medium. At present, we are performing more investigation to optimize the experimental conditions and develop some stabilizer to prevent the Pd/Fe_3O_4 particles from aggregating during reaction and washing.

Acknowledgements

This research was funded by the National Natural Science Foundation of China and the Trans-Century Training Programme Foundation for the Talents by the Ministry of Education of China. Thanks to Z.C. Wang (State Key Lab Palaeobiology and Stratigraphy, Nanjing Institute of Geology and Palaeontology, CAS) for help using transmission electron microscope.

References

[1] A. Roucoux, J. Schulz, H. Patin, Chem. Rev. 102 (2002) 3757–3778.
[2] R.V. Heerbeek, P.C.J. Kamer, P.W.N.M. van Leeuwen, J.N.H. Reek, Chem. Rev. 102 (2002) 3717–3756.
[3] L.K. Yeung, R.M. Crooks, Nano Lett. 1 (2001) 14–17.
[4] K.R. Gopidas, J.K. Whitesell, M.A. Fox, Nano Lett. 3 (2003) 1757–1760.
[5] A.H.M. de Vries, J.P. Floris, L. Schmieder, F.J.P. van de Vondervoort, J.H.M. Mommers, H.J.W. Henderickx, M.A.M. Wallet, J.G. de Vries, Adv. Synth. Catal. 344 (2002) 996–1002.
[6] B.F.G. Johnson, Coord. Chem. Rev. 190–192 (1999) 1269–1285.
[7] Y. Li, X.M. Hong, D.M. Collard, M.A. EI-Sayed, Org. Lett. 2 (2000) 2385–2388.
[8] A. Biffis, M. Zecca, M. Basato, Eur. J. Inorg. Chem. 5 (2001) 1131–1133.
[9] M. Moreno-Mañas, R. Pleixats, Acc. Chem. Res. 36 (2003) 638–643.
[10] M. Králik, A. Biffs, J. Mol. Catal. A Chem. 177 (2001) 113–138.
[11] K. Köhler, R.G. Heidenreich, J.G.E. Krauter, J. Pietsch, Chem. Eur. J. 8 (2002) 622–631.
[12] W. Teunissen, A.A. Bol, J.W. Geus, Catal. Today 48 (1999) 329–336.
[13] M. Ma, Y. Zhang, W. Yu, H.-Y. Shen, H.-Q. Zhang, N. Gu, Colloids Surf. A Physicochem. Eng. Aspects 212 (2003) 219–226.
[14] T. Teranishi, M. Miyake, Chem. Mater. 10 (1998) 594.
[15] C.P. Mehnert, D.W. Weaver, J.Y. Ying, J. Am. Chem. Soc. 120 (1998) 12289–12296.